Water Conserv Sci Eng (2017) 1:249–256
DOI 10.1007/s41101-017-0017-3

ORIGINAL PAPER

Oxidative Degradation of Methylene Blue Using Mn_3O_4 Nanoparticles

A. K. M. Atique Ullah[1,2] · A. K. M. Fazle Kibria[3] · M. Akter[4] · M. N. I. Khan[5] · A. R. M. Tareq[2] · Shakhawat H. Firoz[1]

Received: 20 December 2016 / Revised: 18 January 2017 / Accepted: 19 January 2017 / Published online: 27 January 2017

Abstract Mn_3O_4 nanoparticles were synthesized from one-step reduction of $KMnO_4$ with glycerol at 80 °C. The structural and surface morphological characterizations were carried out using FT-IR, XRD, and FESEM analyses. The elemental composition was evidenced from EDX analysis. XRD analysis showed the tetragonal crystal geometry of Mn_3O_4 nanoparticles with an average crystallite size of ~20 nm. The surface morphology of the Mn_3O_4 nanoparticles was found to be spherical from the FESEM image. The Mn_3O_4 nanoparticles were then tested as a potential oxidant for the decolorization of methylene blue (MB) and found to be capable of N-demethylation of MB forming thionine as the final product, and removing 80% of the dye in approximately 1 h. The decolorization of MB by Mn_3O_4 occurred through a surface mechanism, i.e., formation of surface precursor complex between MB and surface-bound Mn (II, III), where, electron transfer occurs within the surface complex. The effect of suspension pH (3–4 < pH_{pzc}; 5–10 > pH_{pzc}) on MB decolorization was assessed. Suspension pH exerted double-edged effects on MB decolorization by influencing the formation of surface precursor complex, and reducing potential of the system.

Keywords Mn_3O_4 · Methylene blue · Oxidative decolorization · Degradation · Surface precursor

Introduction

During the dyeing process, about 15% of the total world production of dyes is lost and released in the textile effluents [1]. Discharging of the untreated textile effluents into water is one of the major sources of water contamination [2]. The presence of dyes in water reduces light penetration and hinders photosynthesis in aquatic plants [3]. Moreover, many of the dyes are reported to have low biodegradability and are highly carcinogenic [4]. It is, therefore, essential to treat the dye effluents before discharging into the receiving water. As the international environmental standards (ISO 14001:2015) are stringent, a number of technological systems have been recently developed for the removal of organic pollutants, such as dyes. Among them, the most commonly used methods are physical methods such as adsorption [5], biological methods such as biodegradation [6], and chemical methods such as chlorination and ozonation [3].

Advanced oxidation technologies have attracted considerable attention as an emerging technology leading to the total mineralization of most of the organic pollutants. As manganese (Mn) oxides are powerful oxidants having high-reducing potential, for pollution remediation purpose, land-born natural Mn ores, synthetic nascent state Mn oxides, and materials coated/modified with Mn oxides have been tested as oxidants for degradation of organic pollutants [7, 8]. It has already been

✉ A. K. M. Atique Ullah
atique.chem@gmail.com

✉ Shakhawat H. Firoz
shfiroz@chem.buet.ac.bd

[1] Department of Chemistry, Bangladesh University of Engineering and Technology (BUET), Dhaka 1000, Bangladesh

[2] Chemistry Division, Atomic Energy Centre, Bangladesh Atomic Energy Commission, Dhaka 1000, Bangladesh

[3] Nuclear Safety, Security and Safeguards Division, Bangladesh Atomic Energy Commission, Dhaka 1207, Bangladesh

[4] Faculty of Environmental Earth Science, Hokkaido University, Sapporo 060-0810, Japan

[5] Materials Science Division, Atomic Energy Centre, Bangladesh Atomic Energy Commission, Dhaka 1000, Bangladesh

reported that oxides and hydroxides of Mn^{3+} and Mn^{4+} can oxidize a variety of natural and xenobiotic organic compounds such as catechol, quinines, substituted phenols, aromatic amines, pesticides, and explosives (e.g., TNT) [9–13]. Trimanganese tetraoxide (Mn_3O_4) is a mixed oxide of Mn containing both di- and tri-valents of Mn. Reducing potential of Mn_3O_4 is higher than that of other Mn oxides [14].

In view of strong oxidative property of Mn_3O_4, it seems to be interesting to evaluate possible application of Mn_3O_4 as an effective oxidant for the degradation of organic contaminants in water. In the present study, methylene blue (MB) was chosen as a model of organic contaminants as it is the most commonly used dye in the textile industry [15] that can result in permanent burns to the eyes of humans and animals, nausea, vomiting, profuse sweating, mental confusion, and methemoglobinemia [16]. The decolorization of MB using Mn_3O_4 was studied by a number of workers [17, 18]; however, the mechanism of decolorization is not well evident. As a result, a detailed mechanism of the MB decolorization by Mn_3O_4 is inevitable. Consequently, in the present study, it was attempted to evaluate the probable mechanism of MB decolorization along with identifying the intermediate degraded products distinctly, degraded by Mn_3O_4 nanoparticles.

Experimental

Materials and Reagents

The materials and reagents used in this work included potassium permanganate ($KMnO_4$; Merck, India), glycerol ($C_3H_8O_3$; JHD, China), sulfuric acid (H_2SO_4; E. Merck, Germany), sodium chloride (NaCl; E. Merck, Germany), sodium hydroxide (NaOH; BDH), hydrochloric acid (HCl; E. Merck, Germany), methylene blue ($C_{16}H_{18}ClN_3S$; E. Merck, Germany), and methanol (CH_3OH; E. Merck, Germany). All the solutions were prepared with de-ionized water with a resistivity of 18.1 MΩ cm^{-1}. All the chemicals were analytical grade and used without further purification.

Synthesis of Mn_3O_4 Nanoparticles

Mn_3O_4 was prepared by a gel-formation route based on reduction of $KMnO_4$ with glycerol in de-ionized water. The gel precursor was obtained by adding 50 mL 0.4 M glycerol into 100 mL 0.3 M $KMnO_4$ solution drop wise under intensive stirring for 60 ± 10 s. The gel was formed within few seconds. The solution was set aside to gel, undisturbed for 24 h. The gel was heated at 80 °C. Then, the residue was centrifuged and washed with de-ionized water to remove any impurities. Subsequently, the brown product was dried in an oven at 80 °C and stored in a desiccator until its use in the experiments.

Experimental Procedure

X-ray diffraction (XRD) analysis was carried out using X-ray powder diffractometer (Philips PANalytical X'PERT-PRO) equipped with CuKα radiation (1.5418 Å). Crystallographic data (space group) were determined by using HighScore software. The Rietveld refinement technique [19] was used for the identification of crystalline structures of the samples. Surface morphology was carried out by field emission scanning electron microscopy (FESEM, model no. JEOL JSM 7600F). The elemental contents were evidenced by energy dispersive X-ray (EDX) spectroscopy (JEOL JSM 7600F). Fourier transform infrared (FT-IR) spectra were recorded on a spectrometer (Jasco-FTIR-6300) in the wave number range of 4000–400 cm^{-1} on KBr pellets. A UV-vis spectrophotometer (Shimadzu-1800, Japan) was employed to monitor the degradation of MB spectroscopically. The degraded intermediates were monitored by high-performance liquid chromatography (HPLC, Jasco, Japan).

Analytical Methods

Several experimental techniques were employed in order to characterize the Mn_3O_4 nanoparticles. Elemental analysis was performed by EDX spectroscopy method, structural characterization was carried out by using FT-IR spectroscopy and XRD techniques, and surface morphology was monitored using FESEM technique.

The point of zero charge, pH_{pzx}, was determined by acid-base titration method following the procedure adopted previously [20] for a powder sample. In brief, the method is as follows: Exactly 0.5 g of Mn_3O_4 was taken in four different reagent bottles each. Then, 0.1 M 50 mL NaCl solution was added to each bottle. The sample solution was agitated for 24 h at low speed in a shaker. Then, the suspensions were observed in each bottle. Contents of the two bottles were titrated, one with 0.05 M HCl and another with 0.05 M NaOH using a microburette (±0.01 mL). The pH values were noted carefully after addition of each drop of titrant (acid or alkali). Contents of other two bottles were filtered with sintered crucible, and the supernatant thus obtained were titrated with 0.05 M HCl and 0.05 M NaOH separately as before. The experiments were carried out in the same way for the 0.01 M and 0.001 M NaCl solutions.

Decolorization experiment was carried out in a glass beaker containing 100 mL of 30 μM MB dye solution maintaining the medium with pH 3. Then, 10 mg of Mn_3O_4 nanoparticles was added to the dye solution. The mixture was kept undisturbed and allowed to react at room temperature. The progress of decolorizaion was assessed by spectroscopic measurements of the mixture at different time intervals. To investigate the effect of pH on the decolorization process, an experiment was also performed at different pH values keeping the amount of

Mn_3O_4 and the dye concentration constant. In order to analyze the oxidative degradation process of MB, the degraded products were enriched by 100 times. Before analysis, the samples were filtered through millipore discs of 0.45 μm to protect the chromatographic column. HPLC monitoring was carried out using an UV absorbance detector (UV-2070 plus) operated at 280 nm coupled to a C18 Hs (Kyta Tech) column.

Results and Discussion

Characterization of Mn_3O_4 Nanoparticles

EDX Analysis

The chemical composition of the prepared sample was analyzed using EDX analysis as shown in Fig. 1. The lines observed at 5.90, 6.52, and 0.64 keV are associated for K (α, β) and L lines of the Mn element, respectively. The EDX line at 0.52 keV represents K line of the O element. The lines identified in this EDX assigned to Mn and O (Fig. 1) agree with those found in a previous report [21]. The quantification result of the EDX data provided the percentage of each element with energy distribution present in the matrix which allowed us to obtain directly the composition of the samples. Accordingly, the composition of Mn and O in the prepared samples was 71.52 and 24.48%, respectively, indicating the ratio of Mn:O was 3:4. The EDX attributed that the synthesized compound was Mn_3O_4.

FT-IR Analysis

The FT-IR spectrum as shown in Fig. 2 also provided significant qualitative information for the identification of Mn_3O_4 nanoparticles. The spectrum of the Mn_3O_4 nanoparticles displayed three significance peaks in the range of 400–650 cm^{-1}. The vibration frequency located at 618.1 cm^{-1} is a characteristic of Mn-O stretching modes in tetrahedral sites, whereas, the vibration frequency located at 525.5 cm^{-1} corresponds to the distortion vibration of Mn-O in an octahedral environment, and the third vibration band located at 418.5 cm^{-1} is attributed to the vibration of Mn species (Mn^{3+}) in the octahedral site of Mn_3O_4 [22]. Thus, the result further confirmed that the synthesized compound was Mn_3O_4.

XRD Analysis

The typical XRD patterns presented in Fig. 3 were identified as Mn_3O_4 (JCPDS Card No.00-001-1127) with tetragonal crystal structure (space group 141/amd). Crystallite size of the Mn_3O_4 NPs was calculated from diffraction peaks using the Debye-Scherrer approximation [23]. The crystallite sizes measured from the peaks (112, 103, 211, 004, 220, and 224) were averaged to obtain the crystallite size to be 21 ± 2 nm. The values of lattice parameters obtained for each plane were plotted against the Nelson-Riley function, $F(\theta)$ $\left[F(\theta) = \left(\frac{1}{2}\right)[\cos^2\theta/\sin\theta + \cos^2\theta/\theta]\right]$, where θ is the Bragg's angle [24]. A straight line fit was obtained, and the accurate value or the true lattice parameter was determined from the extrapolation of these lines to $F(\theta) = 0$. The lattice parameters of the tetragonal

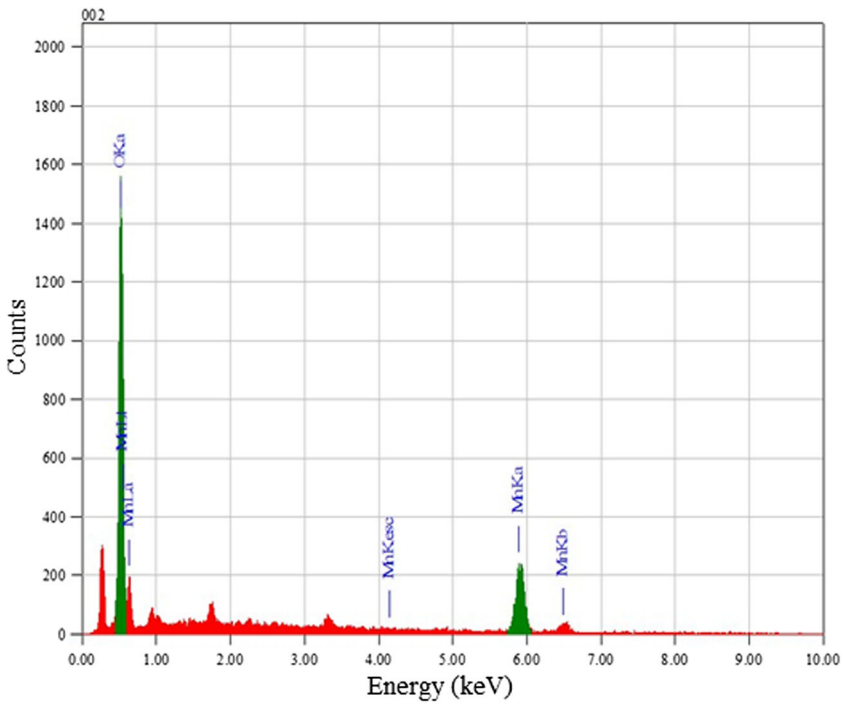

Fig. 1 EDX analysis of Mn_3O_4 nanoparticles

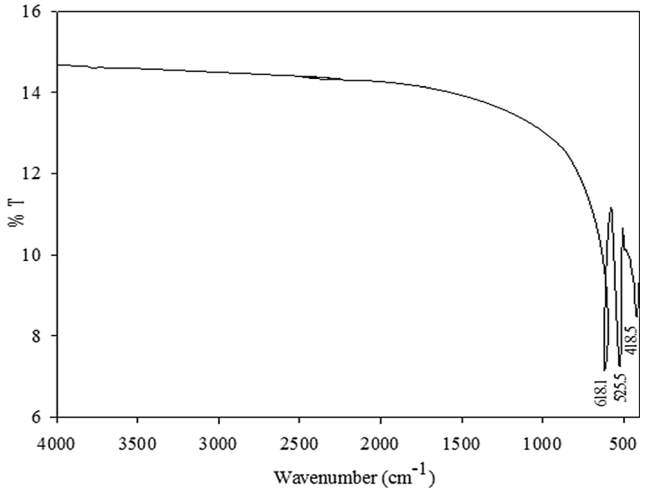

Fig. 2 FT-IR spectrum of Mn_3O_4 nanoparticles

unit cell were found to be a = b = 5.75 Å and c = 9.42 Å, which is in good agreement with previous report [25].

SEM Analysis

Surface morphology of Mn_3O_4 NPs was investigated by virtue of FESEM as shown in Fig. 4. From the image, it can be seen that the Mn_3O_4 particles obtained with a size of several nanometers were aggregated to large spheres. The size of the smaller particles without aggregation was in consistent with that measured from XRD data. It is, indeed, to be of high interest to obtain smaller size particles by preventing aggregation. This might be possible by using some capping agent, e.g., poly vinyl acetate [26] during the synthesis of nanoparticles.

Point of Zero Charge (pH_{pzc})

The point of zero charge (pH_{pzc}) of a solid substance means the pH at which the solid submerged in an electrolyte exhibits

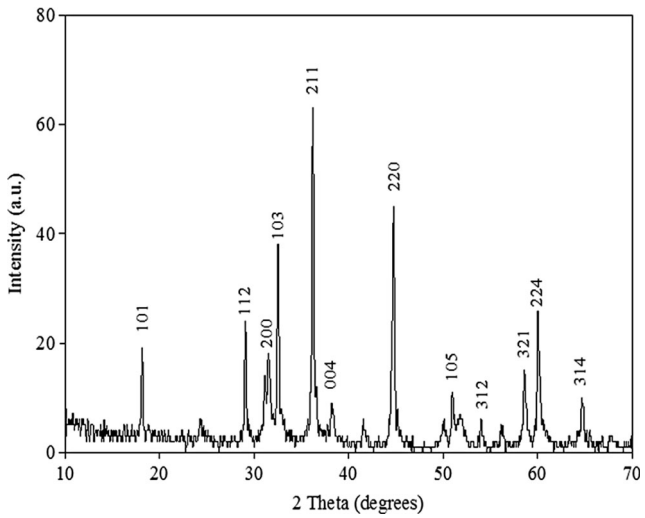

Fig. 3 XRD patterns of Mn_3O_4 nanoparticles

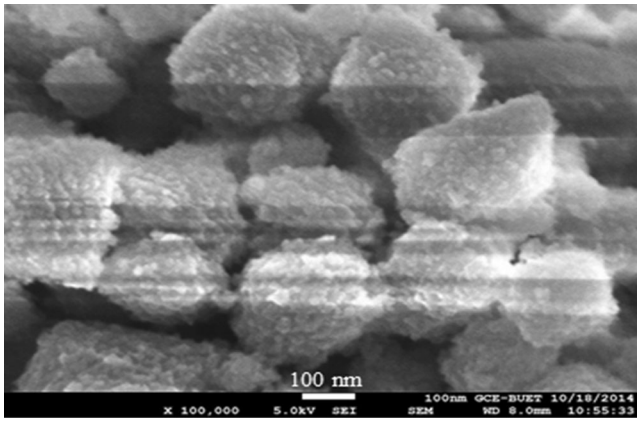

Fig. 4 FESEM image of Mn_3O_4 nanoparticles

zero net electrical charge on the surface. Therefore, the surface properties, viz., adsorption and catalysis of the solid, can be controlled by controlling the pH_{pzc}. Figure 5 shows a typical set of titration curves for the determination of pH_{pzc} of the Mn_3O_4 NPs. The titrations were carried out with NaCl electrolyte having three different ionic strengths, 0.1, 0.01, and 0.001 M. The three titration curves intersected sharply at a common point which indicated the pH_{pzc} of the Mn_3O_4 NPs. In the present study, the pH_{pzc} thus determined for the Mn_3O_4 NPs is 4.5, which is in good agreement with the earlier reported values [27].

Decolorization of MB by Mn_3O_4 Nanoparticles

Spectra of UV-Vis Wavelength Scan

Decolorization of MB could occur through adsorption, catalytic degradation, or oxidation by manganese oxides, since manganese can exist with different oxidation states [28]. The dominated mechanism may depend on the forms of

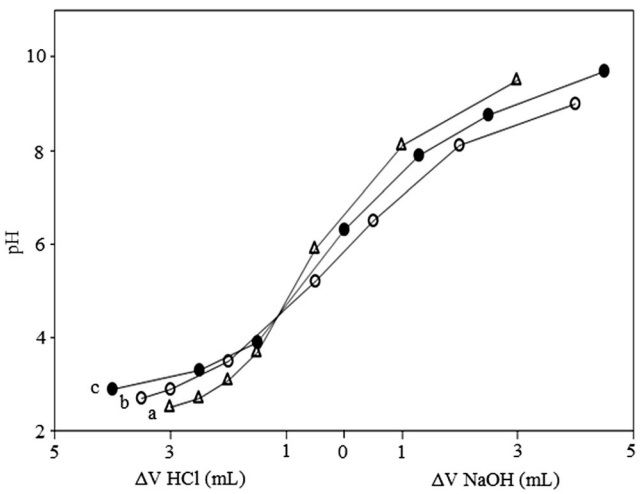

Fig. 5 Typical titration curves for the determination of pH_{pzc} of the Mn_3O_4 nanoparticles. Electrolyte concentrations: (*a*) 0.1 M, (*b*) 0.01 M, and (*c*) 0.001 M

manganese oxides [29] and the nature of their surface sites [30]. The decolorization of MB (30 μM, 100 mL) by Mn_3O_4 nanoparticles (100 mg/L) was investigated spectroscopically. The decolorization of MB by Mn_3O_4 in acidic media was carried out maintaining the media at pH 3 which was lower than that of the pH_{pzc}. Figure 6 shows the UV-vis spectra of the 30 μM MB solution recorded at different times (0 to 240 min). In the spectrum, the characteristic peak of MB at 664 was found which is in good agreement with the reported earlier values [31]. As the reaction time was prolonged, the reaction solution gradually turned colorless and the original absorption maximum at 664 nm was gradually decreased and shifted to shorter wavelength [17, 18] indicating that MB was oxidized by Mn_3O_4. Zaied et al. (2011) found the presence of intermediate reaction products, azure A (AA), azure B (AB), azure C (AC), and thionine (Th) during the degradation of MB using manganese oxide and the corresponding characteristic UV-vis λ_{max} was identified as 628, 638, 618, and 601 nm, respectively [32]. For Mn_3O_4 after 10 min of reaction with MB, λ_{max} became 638, which is similar to λ_{max} of AB; after 20 min, λ_{max} shifted to 628 which is similar to λ_{max} of AA; after 60 min, λ_{max} shifted to 618 which is similar to λ_{max} of AC; and after 240 min, λ_{max} shifted to 603 which is close to λ_{max} of Th. The MB degradation products were further confirmed by HPLC technique.

HPLC Analyses

In order to investigate the oxidative degradation of MB, the composition of MB-degraded intermediates was detected by HPLC. According to the literature [33], the reversed phase eluent of pH 3 buffer and methanol (45:55, *v*/*v*) was used for aqueous solution, and water/methanol (40:60, *v*/*v*) was used for enriched intermediate products. The chromatogram as shown in Fig. 7a is for the original MB solution. The intermediate products obtained from the degradation of MB with Mn_3O_4 at different intervals of reaction time were taken for HPLC analysis, and their corresponding chromatograms are shown in Fig 7b–e. The corresponding chromatograms shown in Fig. 7b–e are for azure A, azure B, azure C, and thionine, respectively. The dye degradation process was repeated for several times, and the degraded intermediates were subjected for HPLC analysis as well. The chromatograms for the degraded products were found to be reproducible. This result suggests that, the four distinct intermediate-degraded products

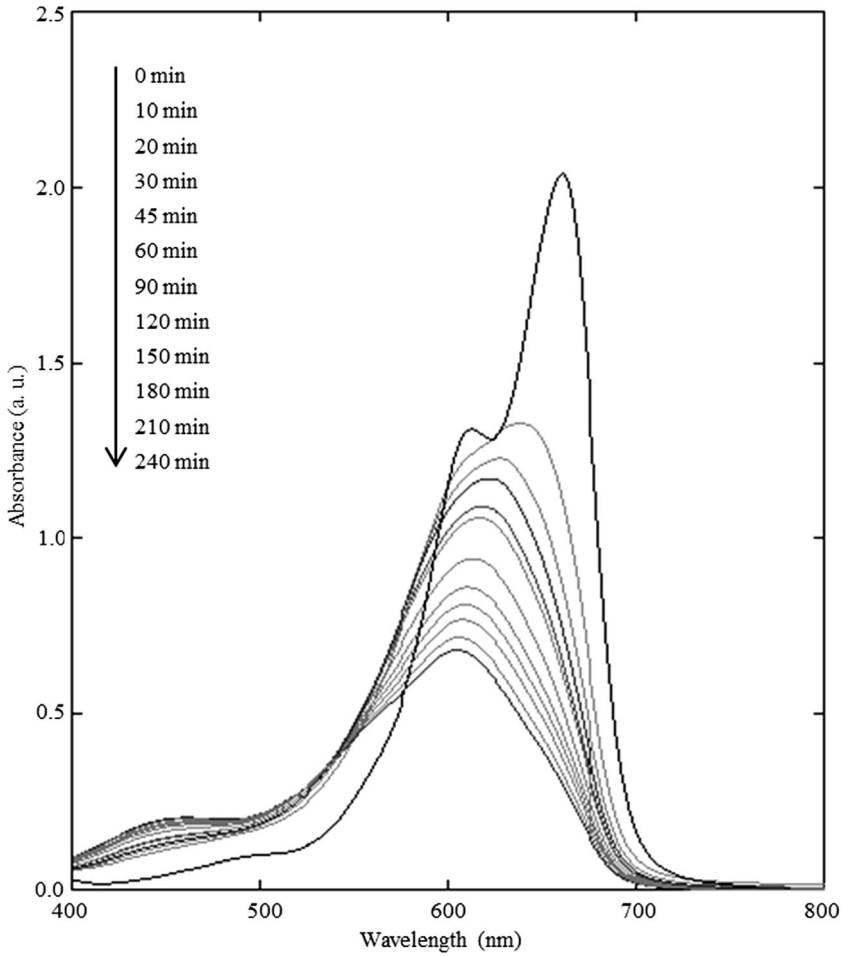

Fig. 6 UV-vis spectra of 30 μM MB dye solution before (0 min) and after (10–240 min) charging the Mn_3O_4 nanoparticles (0.10 g L^{-1} at different time intervals, viz., 10, 20, 30, 45, 60, 90, 120, 150, 180, 210, and 240 min)

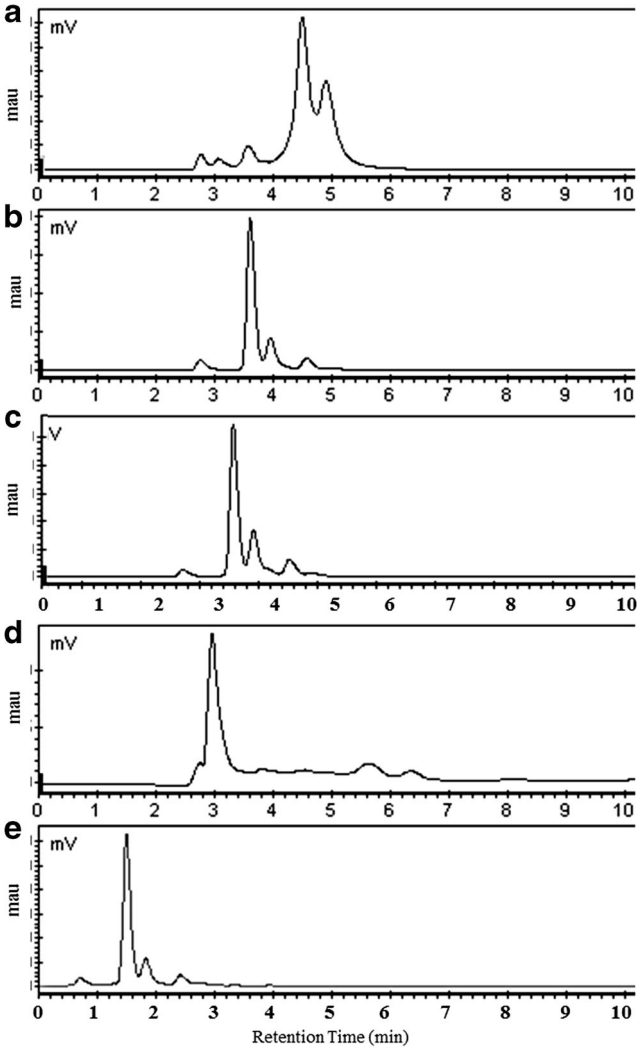

Fig. 7 HPLC analysis of MB degradation products with the initial concentration of 30 μM. (*a*) Original solution in acetonitrile-phosphate buffer (25:75, *v*/*v*). (*b*–*e*) The neutral intermediates enriched by 100 times in methanol/water (60:40, *v*/*v*) eluent

formed during the oxidative degradation of MB with Mn_3O_4 were successfully identified.

Effect of Medium pH on MB Degradation

The effect of medium pH on the MB degradation by Mn_3O_4 nanoparticles was also investigated. The degree of degradation of the sample at different reaction times was calculated according to the following equation:

$$\text{Degree of degradation } (\%) = \frac{A_0(\lambda_{max}) - A(\lambda_{max})}{A_0(\lambda_{max})} \times 100$$

Where, $A_0(\lambda_{max})$ is the initial absorbance and $A(\lambda_{max})$ is the absorbance at time *t* of MB.

Figure 8 shows the degradation of 30 μM MB solution using Mn_3O_4 nanoparticles at (a) pH 3 and (b) pH 4 (both

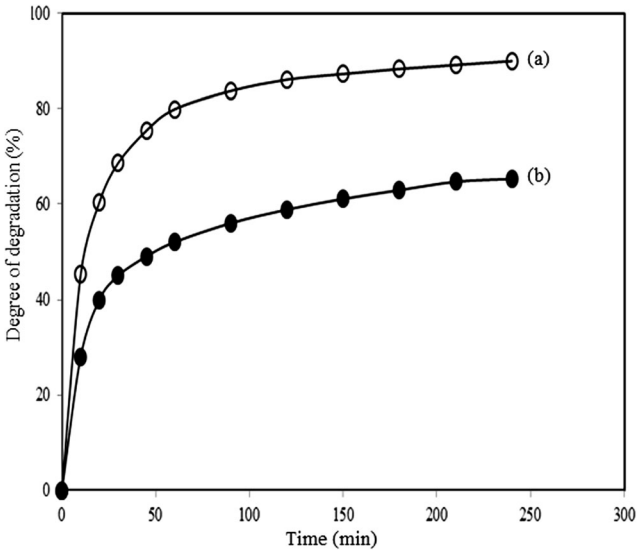

Fig. 8 Effect of medium pH on MB (30 μM) degradation by Mn_3O_4 nanoparticles (0.1 g/L) at (*a*) pH 3 and (*b*) pH 4

are lower than the pH_{pzc}). For 0.1 g/L Mn_3O_4 nanoparticles, above 90% of MB was degraded. When compared to the literature, these results are similar to the ones found for Mn_3O_4/Fe_3O_4 nanocomposites (above 93%), higher than the ones found for ZnS/CdS composites (85%), hollow CdS nanospheres (87%), commercial anatase (73%), ZnO (60%), N-CdS (29%), ZnS (27%), Mn_3O_4/Fe_2O_3 (85%), and photolysis only (21%); and lower than that of G-ZnO (100%) and CdS-6, 8, 18 (above 96%) [34–39]. The results also showed that the degree of degradation was enhanced in lower pH medium. It can be seen from the result that at medium pH

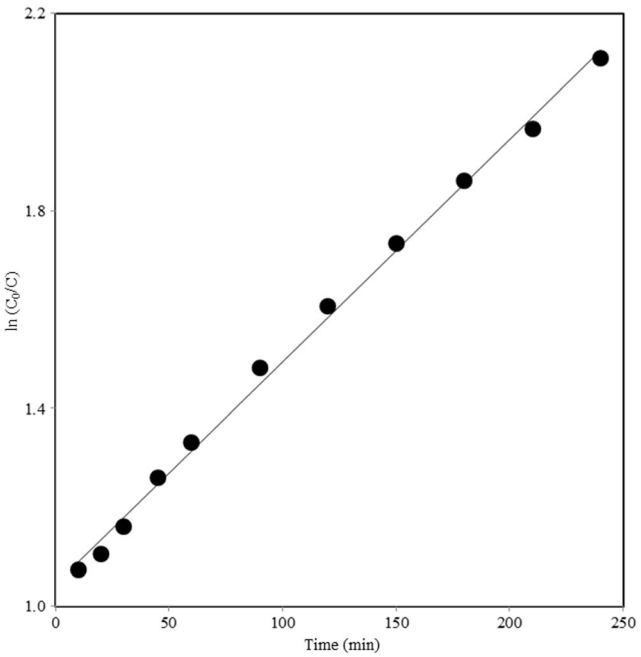

Fig. 9 Pseudo-first-order kinetics model for the degradation of MB (30 μM using Mn_3O_4 nanoparticles) (100 mg/L) at pH 3

greater than 4 (higher than that of pH_{pzc}), MB was not oxidized by Mn_3O_4 [34]. Moreover, in neutral and alkali media, there was hardly any decolorization of MB [17, 18].

It is well established that oxidative degradation of organic pollutants occurred through the formation of surface precursor complex which is closely related to the nature of surface charge. In the present study, the pH_{pzc} of Mn_3O_4 was determined to be 4.5. Theoretically, at pH lower than 4.5, due to protonation, the surface of Mn_3O_4 becomes positively charged and the positive charge of the Mn_3O_4 is increased with the decrease of pH, which does not favor the adsorption of cationic dye MB and formation of surface precursor due to the electrostatic repulsion. At pH higher than 4.5, the surface of Mn_3O_4 becomes negatively charged due to deprotonation and the negative charge is increased with the increase of medium pH, which favors the formation of surface precursor complex due to electrostatic attraction. However, in the present study, experiments show that the degradation of MB is increased with the decrease in medium pH, which suggests that it is due to heterogeneous surface oxidation [40]. Though low pH inhibited the formation of surface precursor complex, but according to Nernst equation, high H^+ concentration could improve the reducing potential of the system resulting in more degradation of MB.

Kinetics of MB Degradation

The oxidative degradation of MB could be quantitatively assessed using reaction kinetics, and possible reaction mechanism can be predicted using the rate expressions obtained from kinetic modeling [40]. The pseudo-first-order kinetics was expressed in terms of Langmuir-Hinshelwood (L-H) model [41]. Figure 9 shows the plot of $\ln C_0/C$ against t where, C represents the concentration of MB at time, t, and C_0 represents the initial concentration of MB. The kinetics of the degradation process fitted to the pseudo-first-order kinetics model well which is in good agreement with the earlier works [12, 13, 42], where the authors reported the oxidative degradation of a number of organic pollutants with Mn oxides. In the present study, the rate constant (k) was found to be 0.0045 min^{-1}. In comparison, the rate constants of MB removal by akhtenskite and birnessite were only 0.0006 and 0.0007 min^{-1}, respectively [43]. Moreover, the higher value of k in our case reveals, the more suitability of the nanoparticles for the degradation of MB [44].

Conclusion

Mn_3O_4 was found to be a promising material for efficient oxidative degradation of methylene blue, and a high extent of mineralization could be achieved. It is evident that about 92% of the dye was removed by Mn_3O_4 nanoparticles following complete demethylation of MB, forming thionine as the final product. The decolorization of MB followed a heterogeneous surface oxidation mechanism. Surface redox takes place immediately after adsorption of dye, and for this reason, it is not likely to determine the saturation concentration of MB on Mn_3O_4 surface and the relative contribution of pure surface adsorption and oxidative degradation to MB decolorization. Suspension pH exerted double-edged effects on the decolorization of MB by influencing the formation of surface precursor complex and reducing potential of the system. At pH less than that of pH_{pzc}, i.e., 4.5, MB decolorization increases with the decrease in suspension pH, whereas, there is hardly any decolorization of MB when suspension pH is greater than that of pH_{pzc} (5–10).

Acknowledgements This work was supported by the CASR of Bangladesh University of Engineering and Technology (BUET) and University Grants Commission (UGC) of Bangladesh.

References

1. Houas A, Lachheb H, Ksibi M, Elaloui E, Guillard C, Herrmann J-M (2001) Photocatalytic degradation pathway of methylene blue in water. Appl Catal B Environ 31:145–157
2. Grau P (1991) Textile industry wastewater treatment. Water Sci Technol 24:97–103
3. Sloker YM, Le Marechal AM (1998) Methods of decolorization of textile wastewater. Dyes Pigments 37:335–356
4. Brown MA, De Vito SC (1993) Predicting azo dye toxicity. Crit Rev Environ Sci Technol 23:249–324
5. Dejohn PB, Hutchins RA (1976) Tex. Chem. Color. 8:69
6. More AT, Vira A, Fogel S (1989) Biodegradation of trans-1, 2-dichloroethylene by methane-utilizing bacteria in an aquifer simulator. Environ Sci Technol 23:403–406
7. Ge J, Qu J (2003) Degradation of azo dye acid red B on manganese dioxide in the absence and presence of ultrasonic irradiation. J Hazard Mater 100:197–207
8. Liu R, Tang H (2000) Oxidative decolorization of direct light red F3B dye at natural manganese mineral surface. Water Res 34:4029–4035
9. Matocha CJ, Sparks DL, Amonette JE, Kukkadapu RK (2001) Kinetics and mechanism of birnessite reduction by catechol. Soil Sci Soc Am J 65:58–66
10. Petrie RA, Grossl PR, Sims RC (2002) Oxidation of pentachlorophenol in manganese oxide suspensions under controlled E h and pH environments. Environ Sci Technol 36:3744–3748
11. Li H, Lee LS, Schulze DG, Guest C (2003) Role of soil manganese in the oxidation of aromatic amines. Environ Sci Technol 37:2686–2693
12. Zhang H, Huang C-H (2005) Oxidative transformation of fluoroquinolone antibacterial agents and structurally related amines by manganese oxide. Environ Sci Technol 39:4474–4483
13. Kang K-H, Lim D-M, Shin H (2006) Oxidative-coupling reaction of TNT reduction products by manganese oxide. Water Res 40: 903–910
14. Reddy KR, DeLaune RD (2008) Biogeochemistry of wetlands: science and applications. CRC Press, New York, NY, USA
15. Zhang L, Nie Y, Hu C, Hu X (2011) Decolorization of methylene blue in layered manganese oxide suspension with H_2O_2. J Hazard Mater 190:780–785

16. Rafatullah M, Sulaiman O, Hashim R, Ahmed A (2010) Adsorption of methylene blue on low-cost adsorbents: a review. J Hazard Mater 177:70–80
17. Zhang P, Zhan Y, Cai B, Hao C, Wang J, Liu C, Meng Z, Yin Z, Chen Q (2010) Shape-controlled synthesis of Mn_3O_4 nanocrystals and their catalysis of the degradation of methylene blue. Nano Res 3:235–243
18. Chowdhury A-N, Azam MS, Aktaruzzaman M, Rahim A (2009) Oxidative and antibacterial activity of Mn_3O_4. J Hazard Mater 172: 1229–1235
19. Rietveld HM (1969) A profile refinement method for nuclear and magnetic structures. J Appl Crystallogr 2:65–71
20. Huang CP, Ostovic FB (1978) Removal of cadmium (II) by activated carbon adsorption. J Environ Eng Div ASCE 104:863–878
21. Nelsona AJ, Reynoldsa JG, Roosb JW (2002) Comprehensive characterization of engine deposits from fuel containing MMT. Sci Total Environ 295:183–205
22. Chiu VQ, Hering JG (2000) Arsenic adsorption and oxidation at manganite surfaces. 1. Method for simultaneous determination of adsorbed and dissolved arsenic species. Environ Sci Technol 34: 2029–2034
23. Scherrer P (1918) Bestimmung der Grösse und der InnerenStruktur von KolloidteilchenMittelsRöntgenstrahlen, Nachrichten von der Gesellschaft der Wissenschaften, Göttingen *Mathematisch-PhysikalischeKlasse*, 2:98–100
24. Nelson JB, Riley DP (1945) An experimental investigation of extrapolation methods in the derivation of accurate unit-cell dimensions of crystals. Proc Phys Soc 57:160–177
25. Augustin M, Fenske D, Bardenhagen I, Westphal A, Knipper M, Plaggenborg T, Kolny-Olesiak J, Parisi J (2015) Manganese oxide phases and morphologies: a study on calcination temperature and atmospheric dependence. Beilstein J Nanotechnol 6:47–59
26. Dharmaraj N, Prabu P, Nagarajan S, Kim CH, Park JH, Kim HY (2006) Synthesis of nickel oxide nanoparticles using nickel acetate and poly (vinyl acetate) precursor. Mater Sci Eng B 128:111–114
27. Durmus Z, Tomas M, Baykal A, Kavas H, Altincekic TG, Toprak MS (2010) The effect of neutralizing agent on the synthesis and characterization of Mn_3O_4 nanoparticles. Russ J Inorg Chem 55: 1947–1952
28. Khan W-H, Chan Y-C (2012) pH-dependent mechanism of methylene blue reacting with tunneled manganese oxide pyrolusite. J Hazard Mater 239-240:152–159
29. Suib SL (2008) Porous manganese oxide octahedral molecular sieves and octahedral materials. Acc Chem Res 41:479–487
30. Trasatti S (1987) Oxide/aqueous solution interfaces, interplay of surface chemistry and electrocatalysis. Mater Chem Phys 16:157–174
31. Zhang TY, Oyama T, Aoshima A, Hidaka H, Zhao JC, Serpone N (2001) Photooxidative N-demethylation of methylene blue in aqueous TiO_2 dispersions under UV irradiation. J Photochem Photobiol A 140:163–172
32. Zaied M, Peulona S, Bellakhal N, Desmazieresd B, Chaussea A (2011) Studies of N-demethylation oxidative and degradation of methylene blue by thin layers of birnessite electrodeposited onto SnO_2. Appl Catal B Environ 101:441–450
33. Lin J, Zong R, Zhou M, Zhu Y (2009) Photoelectric catalytic degradation of methylene blue by C_{60}-modified TiO_2 nanotube array. Appl Catal B Environ 89:425–431
34. Silva GC, Ciminelli VST, Ferreira AM, Pissolati NC, Pavia PRP, Lopez JL (2014) A facile synthesis of Mn_3O_4/Fe_3O_4 superparamagnetic nanocomposites by chemical precipitation: characterization and application in dye degradation. Mater Res Bull 49:544–551
35. Liu S, Li H, Yan L (2013) Synthesis and photocatalytic activity of three-dimensional ZnS/CdS composites. Mater Res Bull 48:3328–3334
36. Zhang W-M, Jiang Y-Q, Cao X-Y, Chen M, Ge D-L, Sun Z-X (2013) Synthesis of pore-variable mesoporous CdS and evaluation of its photocatalytic activity in degrading methylene blue. Mater Res Bull 48:4379–44384
37. Lin G, Zheng J, Xu R (2008) Template-free synthesis of uniform CdS hollow nanospheres and their photocatalytic activities. J Phys Chem C 112:7363–7370
38. Wei A, Xiong L, Sun L, Liu Y, Li W, Lai W, Liu X, Wang L, Huang W, Dong X (2013) One-step electrochemical synthesis of a graphene–ZnO hybrid for improved photocatalytic activity. Mater Res Bull 48:2855–2860
39. Li X, Gao Y, Yu L, Zheng L (2010) Template-free synthesis of CdS hollow nanospheres based on an ionic liquid assisted hydrothermal process and their application in photocatalysis. J Solid State Chem 183:1423–1432
40. Zhu M-X, Wang Z, Zhou L-Y (2008) Oxidation decolorization of methylene blue using pelagite. J Hazard Mater 150:37–45
41. Luo X, Zhang S, Lin X (2013) New insights on degradation of methylene blue using thermocatalytic reactions catalyzed by low-temperature excitation. J Hazard Mater 260:112–121
42. Laha S, Luthy RG (1990) Oxidation of aniline and other primary aromatic amines by manganese dioxide. Environ Sci Technol 24: 363–373
43. Wang X, Mei L, Xing X, Liao L, Lv G, Li Z (2014) Mechanism and process of methylene blue degradation by manganese oxides under microwave irradiation. Appl Catal B Environ 160-161:211–216
44. Luan J, Hu Z (2012) Synthesis, property characterization, and photocatalytical activity of novel visible light-responsive photocatalyst Fe2BiSbO7. Int J Photoenergy 2012:1–11